Chemistry & Biology
Article

Targeting NAD Biosynthesis in Bacterial Pathogens: Structure-Based Development of Inhibitors of Nicotinate Mononucleotide Adenylyltransferase NadD

Leonardo Sorci,[1] Yongping Pan,[2] Yvonne Eyobo,[3] Irina Rodionova,[1] Nian Huang,[3] Oleg Kurnasov,[1] Shijun Zhong,[2] Alexander D. MacKerell, Jr.,[2,*] Hong Zhang,[3,*] and Andrei L. Osterman[1,*]
[1]Burnham Institute for Medical Research, La Jolla, CA 92037, USA
[2]Department of Pharmaceutical Sciences, School of Pharmacy, University of Maryland, Baltimore, MD 21201, USA
[3]Department of Biochemistry and University of Texas Southwestern Medical Center, Dallas, TX 75390, USA
*Correspondence: amackere@rx.umaryland.edu (A.D.M.), zhang@chop.swmed.edu (H.Z.), osterman@burnham.org (A.L.O.)
DOI 10.1016/j.chembiol.2009.07.006

SUMMARY

The emergence of multidrug-resistant pathogens necessitates the search for new antibiotics acting on previously unexplored targets. Nicotinate mononucleotide adenylyltransferase of the NadD family, an essential enzyme of NAD biosynthesis in most bacteria, was selected as a target for structure-based inhibitor development. Using iterative in silico and in vitro screens, we identified small molecule compounds that efficiently inhibited target enzymes from *Escherichia coli* (*ec*NadD) and *Bacillus anthracis* (*ba*NadD) but had no effect on functionally equivalent human enzymes. On-target antibacterial activity was demonstrated for some of the selected inhibitors. A 3D structure of *ba*NadD was solved in complex with one of these inhibitors (*3_02*), providing mechanistic insights and guidelines for further improvement. Most importantly, the results of this study help validate NadD as a target for the development of antibacterial agents with potential broad-spectrum activity.

INTRODUCTION

The versatility and resourcefulness of microbes in developing resistance to various therapies are widely recognized. Although chemical modifications of existing drugs and the development of novel inhibitors against a handful of previously established targets have proven to be successful in the short term, it is also apparent that new drug targets need to be explored to maintain and extend efficacious antibacterial therapy in the long run (McDevitt and Rosenberg, 2001). The need for new targets is further exacerbated by the emergence of bacterial pathogens with natural resistance to existing antibiotics and by a potential threat of pathogens with engineered antibiotic resistance.

Previous studies implicated NAD(P) biosynthesis as a promising, albeit relatively unexplored, target pathway for the development of novel antimicrobial agents (Gerdes, et al., 2002; Osterman and Begley, 2007; Sassetti, et al., 2003). Cofactors of the NAD pool are indispensable as they are involved in hundreds of redox reactions in the cell. Additionally, NAD is utilized as a cosubstrate by a number of nonredox enzymes (e.g., by bacterial DNA ligases and protein deacetylases of the CobB/Sir2 family). This dictates the need to maintain NAD homeostasis via its active resynthesis and recycling of NAD degradation products. Recently, a number of insightful reviews have emphasized the potential of NAD(P) biosynthetic enzymes as drug targets for the treatment of cancer, autoimmune diseases, and neurodegenerative disorders (Chen, et al., 2008; Khan, et al., 2007; Lau, et al., 2009; Magni, et al., 2009). Although the early steps in NAD biogenesis and recycling vary substantially between species, the enzymes driving the downstream conversion of nicotinic acid mononucleotide (NaMN) to NAD and NADP are present in nearly all analyzed bacterial genomes (Osterman and Begley, 2007; Sorci, et al., 2009) (Figure 1). Therefore, all three enzymes of this pathway—NaMN adenylyltransferase (EC 2.7.7.18), NAD synthetase (EC 6.3.1.5), and NAD kinase (EC 2.7.1.23)—encoded by the conserved genes *nadD*, *nadE*, and *nadK*, represent promising broad-spectrum antibacterial targets. The observed essentiality of the respective genes is due to the bacteria being unable to uptake phosphorylated pyridine nucleotides (Gerdes, et al., 2002; Osterman and Begley, 2007). Recent progress in the development of inhibitors targeting the last two enzymes, NadE (Velu, et al., 2003; Velu, et al., 2005; Velu, et al., 2007) and NadK (Bonnac, et al., 2007; Poncet-Montange, et al., 2007), provides additional validation of NAD biosynthesis as a target pathway. We have selected the NadD enzyme as a target for the development of specific inhibitors on the basis of a number of criteria such as essentiality, broad conservation, and structure-function distinction from its human counterpart (Gerdes, et al., 2002; Zhou, et al., 2002).

NadD converts NaMN, the first intermediate shared by the most common de novo and salvage/recycling routes, to nicotinic acid adenine dinucleotide (NaAD) (Figure 1). Therefore, this enzyme should be indispensable in all bacterial species that utilize one or both of these routes for NAD biosynthesis. This is consistent with gene essentiality data for a number of bacterial species (as reviewed in Gerdes, et al., 2006 and Gerdes, et al., 2002). For example, the *nadD* gene was shown to be essential for survival in *Staphylococcus aureus* and *Streptococcus pneumoniae* that are fully dependent on niacin salvage (via PncA-PncB route). It is also essential in *Escherichia coli* and *Mycobacterium tuberculosis*, organisms that harbor both the de novo

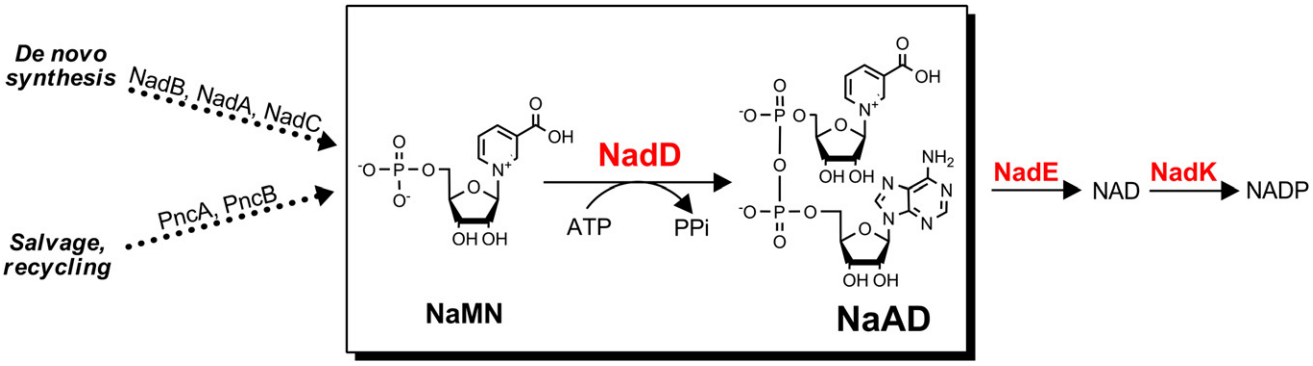

Figure 1. NAD(P)-Biosynthesis Pathways in Bacteria

NadD target enzyme is conserved in most bacteria. NaMN, a common biosynthetic intermediate in the salvage and de novo NAD biosynthetic pathways, is the substrate for NadD. The ATP substrate acts as the adenylyl moiety donor for NaMN, yielding PPi and NaAD. The latter product is then amidated (and phosphorylated) to give NAD and NADP.

(NadB-NadA-NadC) and the salvage pathways. Remarkably, it has been recently demonstrated that NAD downstream pathway holds as an attractive target in both actively growing and nonreplicating pathogens (Boshoff, et al., 2008). NadD is present in nearly all important pathogens with only a few exceptional cases, such as *Haemophilus influenzae*, which lacks most of NAD biosynthetic machinery and is dependent on salvage of the so-called V-factors (Gerlach and Reidl, 2006).

Many representatives of the NadD family from pathogenic and model bacteria have been characterized mechanistically and structurally (Han, et al., 2006; Lu, et al., 2008; Olland, et al., 2002; Sershon, et al. 2009; Yoon, et al., 2005; Zhang, et al., 2002). All of these enzymes have a strong substrate preference for NaMN over its amidated analog, NMN. On the other hand, all three isoforms of the functionally equivalent human enzyme (*hs*NMNAT-1, *hs*NMNAT-2, and *hs*NMNAT-3) have an almost equal catalytic efficiency for either substrate, NaMN or NMN (Berger, et al., 2005; Sorci, et al., 2007). The observed difference in substrate specificity reflects the dual physiological role of the human enzyme (hereafter referred to as *hs*NMNAT) in the adenylation of both intermediates contributing to NAD biogenesis (Lau, et al., 2009; Magni, et al., 2008). Notably, among the three bacterial enzymes of the target pathway shown in Figure 1, NadD has the lowest sequence similarity to its human counterparts (Gerdes, et al., 2002). Comparative analysis of 3D structures of bacterial NadD and *hs*NMNAT revealed significant differences between their active site conformations (Zhou, et al., 2002), which are likely responsible for their distinct substrate specificities, thus opening an opportunity for selective targeting.

The goals of the present study are to use a structure-based approach to identify low-molecular-weight compounds that selectively inhibit representative NadD enzymes, and to test whether such inhibitors suppress the growth of model gram-positive and gram-negative bacteria. Among the most important results is the validation of the NadD family as a druggable target whose specific inhibition leads to the suppression of bacterial growth in culture. Detailed interactions between NadD enzyme from *Bacillus anthracis* (*ba*NadD) and one of the selected inhibitors were revealed by the X-ray cocrystal structure, information that will be instrumental in lead optimization and in development of drug prototypes.

RESULTS

An overview of the structure-based approach applied in this study for NadD inhibitor discovery is summarized in Figure 2. In silico screening of the large virtual library of low-molecular-weight compounds to identify potential NadD inhibitors was performed using the *ec*NadD structural template. Of the ~500 top-ranking in silico hits, 307 commercially available compounds were subjected to in vitro primary testing for inhibition of two representative target enzymes, *ec*NadD and *ba*NadD. A series of analogs of three high-ranking compounds of distinct chemotypes (***1***, ***3***, and ***15***) active against both target enzymes were characterized in more detail by both enzymatic and cell-based assays. A cocrystal structure of *ba*NadD in complex with one of the inhibitors, ***3_02***, revealed atomic details of its interactions with the enzyme active site, providing guidelines for future structure-based inhibitor optimization.

In Silico Screening of the Compound Library

The design of the template for in silico screening was based on the 3D structure of *ec*NadD reported in our earlier study (Zhang, et al., 2002). The targeted binding pocket encompassed the nicotinosyl binding site (near residues Asn40, Thr85, Phe104, and Ile106 in *ec*NadD) as well as the catalytic site near the conserved (H/T)xGH motif (around Phe8, Gly10, and His19). The initial screen of ~1 million compounds targeted a single conformation of *ec*NadD in apo-form, which was followed by two rounds of secondary screens. In the first round, 20,000 top-scoring compounds selected in the initial screen were rescreened against two additional apo-*ec*NadD conformations obtained from the 1k4k crystal structure (Zhang, et al., 2002). In the second round, 50,000 compounds from the initial screen were docked onto five *ec*NadD conformations obtained from an MD simulation. Of the 500 top-scoring compounds selected by these two screens, a total of 307 were purchased from vendors and were subjected to experimental testing of their NadD inhibitory activity (see Table S1 available online).

Experimental Testing of NadD Inhibitors

To evaluate the compounds obtained from virtual screening, we experimentally tested their inhibitory activity against two

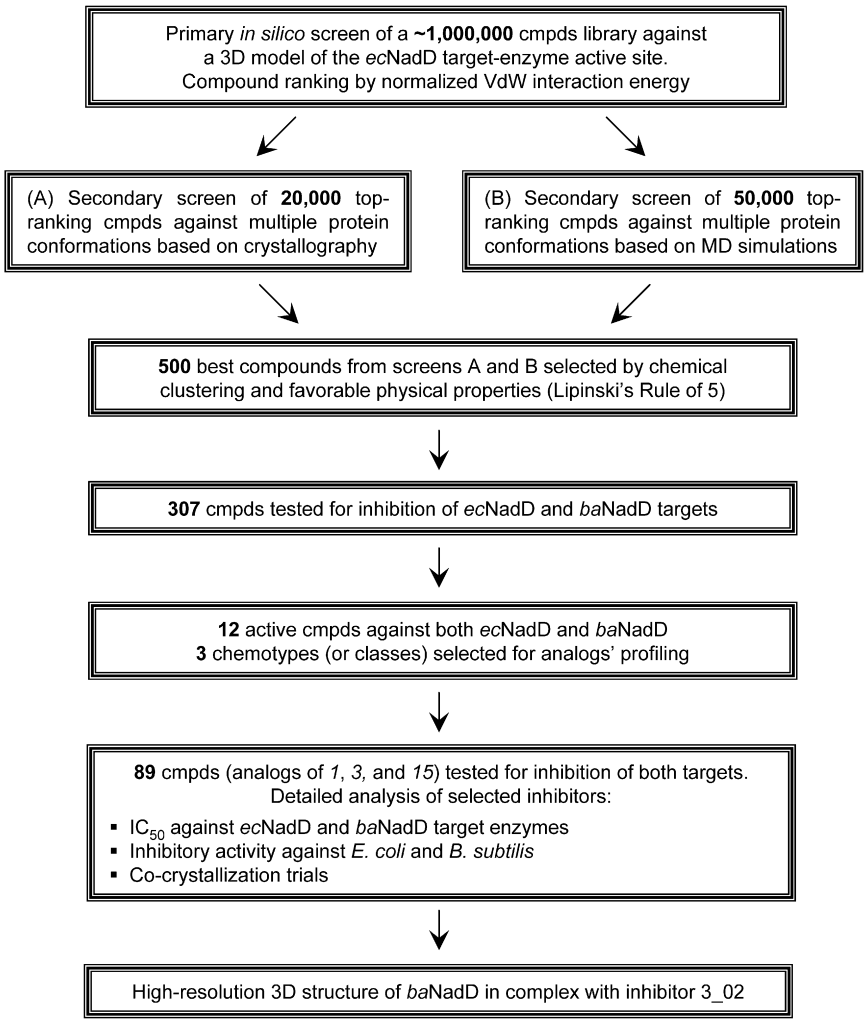

Figure 2. Flowchart of the Structure-Based Approach for Developing Bacterial NadD Inhibitors

representative NadD target enzymes, from the model gram-negative bacterium *E. coli* and from the gram-positive pathogen *B. anthracis*. Both recombinant enzymes were overexpressed in *E. coli* and were purified, and their steady-state kinetic parameters were obtained using a standard coupled assay (Kurnasov, et al., 2002). An extensive kinetic analysis of *ba*NadD enzyme, which included detection and exploration of negative cooperativity, was recently published (Sershon, et al., 2009). The results of our previously reported kinetic analysis of this enzyme, albeit less detailed, yielded comparable steady state parameters that reflect strong preference for NaMN over NMN (Sorci, et al., 2009). A similar preference was observed for *ec*NadD (Table S2). The experimental testing of selected compounds for their ability to inhibit NaMNATase activity of NadD enzymes was performed in the 96-well microtiter plate format using a colorimetric end-point assay, which includes an enzymatic conversion of the released PPi to Pi and a chromogenic reaction with the ammonium molybdate/malachite green reagent (Cogan, et al., 1999).

At this stage of analysis, we aimed to detect inhibitors with moderate affinity (e.g., IC_{50} at least 100 μM or better). Therefore, for each of the two enzymes, the testing was performed in the presence of compounds at 50–100 μM. The results of primary testing of all 307 compounds against both enzymes are shown in Table S1. At the 20% inhibition threshold, this method identified 38 *ec*NadD inhibitors. Remarkably, the *ba*NadD enzyme showed on average a two-fold higher susceptibility to inhibition, yielding 77 compounds at the same threshold. An appreciable correlation across the entire set of 307 analyzed compounds could be observed in their inhibitory properties against both enzymes (Table S1). This trend can be best illustrated by the comparison of two sets of ~10% top-ranking *ec*NadD and *ba*NadD inhibitors revealing that nearly one-third of them are shared between both sets (the estimated probability to get at least 12 random matches is $3 \cdot 10^{-12}$, see Supplemental Data). This observation indicated that the applied in silico screening strategy was indeed successful in targeting NadD active-site components conserved between quite divergent representatives of this enzyme family. By combining this strategy with the parallel experimental testing of compounds against two divergent target enzymes, we were able to identify 12 potentially broad-spectrum NadD inhibitors. Three of these inhibitors (***1***, ***3***, and ***15***) with distinct scaffolds were selected for further analysis, including characterization of their analogs by enzymatic and cell-based assays and cocrystallization trials.

Selection and Comparative Analysis of NadD Inhibitor Analogs

To validate and further explore the utility of the three selected chemotypes, structurally similar and commercially available analogs of compounds ***1***, ***3***, and ***15*** were identified using chemical fingerprint–based similarity analysis (Butina, 1999; Godden, et al., 2005). For each of the primary compounds, 15 to 40 analogs were purchased and analyzed by the same inhibitory assay. Inhibitory activity above a 20% threshold against at least one of the analyzed NadD enzymes was confirmed for 66 of the 89 analogs (Table S3). For example, of the 29 analogs of compound ***3***, 23 were active against *ec*NadD and 24 were active against *ba*NadD, whereas all 18 analogs of compound ***1*** turned out to be inhibitors of both enzymes. Notably, among 42 analogs of compound ***15***, 23 compounds were confirmed as *ba*NadD inhibitors, but only 2 compounds had an appreciable inhibitory effect on *ec*NadD.

Overall, an observed frequent occurrence of analogs of compounds ***1*** and ***3*** that are active against both divergent members of NadD family supports the possibility of developing

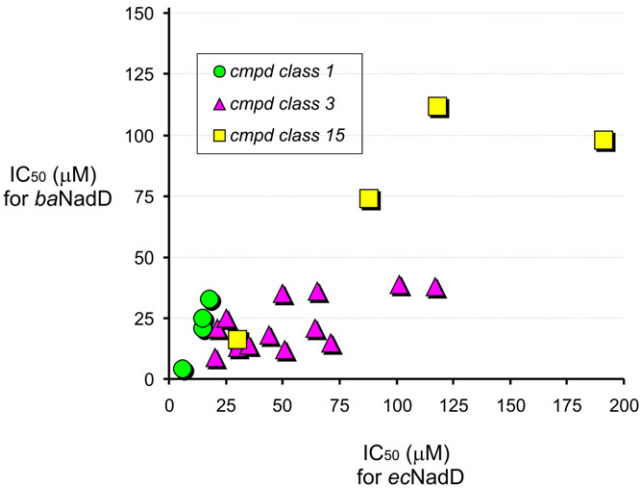

Figure 3. Correlation Analysis of IC_{50} Values for Classes *1*, *3*, and *15* Compounds

The analysis was restricted to compounds with IC_{50} values <0.2 mM and was computed on the assumption that both IC_{50} values for *E. coli* and *B. anthracis* NadDs follow a Gaussian distribution.

broad-spectrum NadD inhibitors. Although all the analyzed analogs were selected only on the basis of structural similarity (without any attempts of their rational improvement), many of them displayed a moderate improvement of inhibitory properties, compared with the original compounds. For example, 10 analogs of compounds ***1*** and ***3*** had improved activity against *ec*NadD, and 22 had improved activity against *ba*NadD, pointing the possibility towards their further optimization. IC_{50} values against *ec*NadD and *ba*NadD determined for a subset of 33 compounds representing all three chemotype ranged from low micromolar to >200 μM (Table S3). Comparative analysis of these data revealed an appreciable correlation ($r = 0.79$) of the inhibitory properties of these compounds against both target enzymes over the entire subset (Figure 3). The strongest correlation was observed for the compounds from the most active class ***1*** ($r = 0.98$).

To assess potential selectivity of these inhibitors against bacterial targets, several of the most active representatives of each chemotype were tested for their ability to inhibit human counter-target enzymes (*hs*NMNAT-1-3). These assays were performed at 100 μM concentration of the compounds (i.e., in the conditions leading to > 90% inhibition of bacterial NadD enzymes). Remarkably, none of the tested compounds displayed any appreciable inhibitory activity against the three human isozymes (<5% for *hs*NMNAT-1 and *hs*NMNAT-3, and <10% for *hs*NMNAT-2). These compounds displayed the same efficacy and specificity when tested at a higher concentration of BSA (1 mg/ml) in the assay, which is a common test to eliminate promiscuous inhibitors (Coan and Shoichet, 2007; Shoichet, 2006). Overall, the observed antibacterial selectivity and versatility of the analyzed inhibitors further support NadD as a promising target for the development of potential broad-spectrum antibiotics.

Effects of NadD Inhibitors on Bacterial Cell Growth

The antibacterial activity of selected NadD inhibitors was assessed by their ability to suppress the growth of model gram-negative (*E. coli*) and gram-positive (*B. subtilis*) bacteria in liquid culture. To establish conditions potentially maximizing the effect of NadD inhibition in an *E. coli* model, we used a Δ*nadA* mutant strain with disrupted de novo NAD synthesis. To further restrict the flux of NaMN (the committed substrate of the NadD target enzyme), we performed the growth studies on the experimentally established lowest concentration of Nam (0.4 μM) supporting the growth of this diagnostic strain on minimal media. In these conditions, many of the selected NadD inhibitors of classes ***1*** and ***3*** showed an appreciable growth suppression effect at 100 μM (Figure 4A and Table S3). To assess the extent of "on-target" (NadD-dependent) versus "off-target" (nonspecific) antibacterial effects of these compounds, we used a derivative of the same *E. coli* strain containing an overexpression plasmid vector with the *E. coli nadD* gene. The growth of this strain in the presence of selected inhibitors was compared to an isogenic control strain containing the same plasmid vector overexpressing a housekeeping *gapA* gene (unrelated to NAD synthesis). As shown in Figures 4C and 4D, overexpression of *ec*NadD suppressed the antibacterial activity of the tested representatives of NadD inhibitors of classes ***1*** and ***3***. On the other hand, the bactericidal effect of the compound ***15_11*** (Table 1) was essentially the same in both the NadD-overexpressing and control strain (Figure S3), suggesting that this effect is largely nonspecific (NadD independent). An alternative interpretation that the on-target activity of ***15_11*** is too high to be suppressed by NadD overexpression appears unlikely, as the in vitro inhibitory properties of this compound are below average ($IC_{50,\ ecNadD}$ ~200 μM). On the basis of the structure of this compound, one may expect its hydrolysis in the medium to benzoate, a compound known to have a general and nonspecific antibacterial activity. On the basis of a combination of these observations and considerations, we excluded compounds of the class ***15*** from further analysis. An appreciable antibacterial activity was also observed for several analogs of compounds ***1*** and ***3*** against the model gram-positive bacteria *B. subtilis* (Figure 4B and Table S3). Interestingly, the antibacterial effect of tested compounds in *B. subtilis* was manifested by delayed growth, in contrast to *E. coli*. where it was largely a decreased final cell density (Figure 4B). Although establishing a rationale for this difference and confirming the actual target in gram-positive bacteria remain to be accomplished, the growth-suppression data shown in Figure 4 and Table S3 indicate that NadD inhibitors may indeed function as broad-spectrum antibiotics.

We further determined MIC for active compounds ***3_02***, ***3_05***, ***3_15***, ***3_23***, and ***1_03*** against *B. anthracis* sterne, *B. subtilis*, and *E. coli*. A general correlation was observed between NadD inhibition and antibacterial activity, although it was less pronounced in *E. coli* (Table 1). Cell wall impermeability of gram-negative bacteria could be a major determinant of such weaker susceptibility. Notably, some of the less efficient *ec*NadD inhibitors (e.g., ***3_23*** and ***15_11***) showed a relatively strong antibacterial activity against *E. coli*. This observation may reflect the existence of additional targets affected by these compounds (see also Figure S3), nonspecific or even sharing some common features with NadD (Moro, et al., 2009).

Mechanistic and Structural Analysis of NadD Inhibition

Representatives of both classes ***1*** and ***3*** of efficient NadD inhibitors were selected for detailed kinetic characterization and

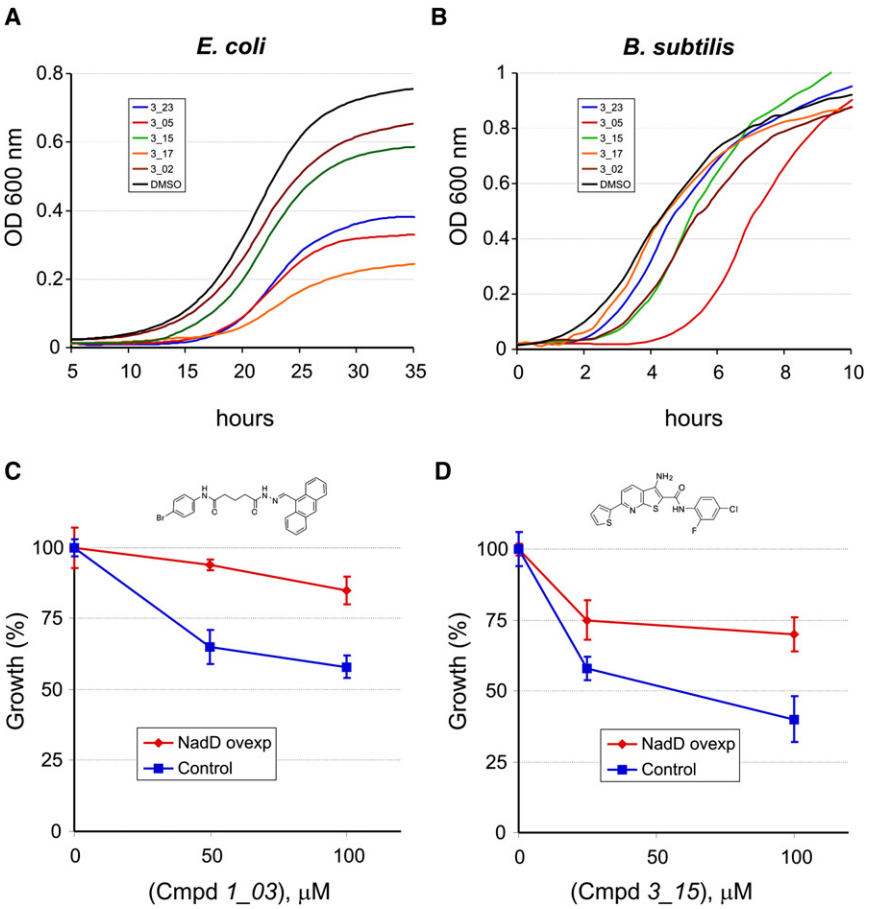

Figure 4. Growth Inhibition of Model Bacteria and Validation of NadD Target

(A and B) Effect of inhibitors of class ***3*** (100 μM for *E. coli* and 50 μM for *B. subtilis*) on cell growth as reflected in changes of the optical density at 600 nm.

(C and D) Overexpression of NadD in *E. coli* Δ*nadA, nadD*$^+$ (red) increases resistance to inhibitors ***3_15*** (C) and ***1_03*** (D) compared to a control strain overexpressing enzyme GapA, unrelated to NAD (blue). Inhibitors were tested at ≤100 μM because of solubility issues at higher concentrations. Results are shown as mean ± SD and are representative of two or more experiments.

cocrystallization trials. Apparent steady-state inhibitory parameters were obtained for compounds ***1_02*** and ***3_02*** against *ec*NadD and *ba*NadD with respect to each substrate ATP and NaMN (Table 2 and Figure S1). A preliminary assessment of all kinetic profiles revealed a mixed-type inhibition, as indicated by $\alpha > 1$ values obtained by fitting initial rates to a general inhibition model (see Equation 2 in Experimental Procedures). Despite the observed complex behavior preventing a straightforward mechanistic interpretation, the obtained data showed a substantial similarity in the inhibitory properties of both compounds with respect to both target enzymes.

The 3D structure of the complex of *ba*NadD, cocrystallized with compound ***3_02*** and solved at 2.0 Å resolution, revealed its binding in the active-site area mostly through van der Waals interactions. The planar compound stacks against two aromatic residues, Trp116 and Tyr112 (*ba*NadD numbering), and is also in contact with Met109 and Phe103 (Figure 5A). Although there are a few water-mediated indirect interactions between ***3_02*** and the enzyme, there is no direct intermolecular hydrogen-bond in-teraction. A comparison with the 3D structure of *ba*NadD complexed with the NaAD product solved in this study at 2.2 Å resolution and with the recently reported apo-*ba*NadD structures (Lu, et al., 2008; Sershon, et al., 2009) provided additional insights to the structural mechanism of inhibition. This comparison revealed that the bound compound ***3_02*** partially overlaps with the nicotinosyl binding site and would interfere with NaMN substrate binding (Figure 5B). In particular, inhibitor binding would potentially block the critical stacking interaction between the side-chain of the conserved Trp116 residue with the pyridine ring of the NaMN substrate (Olland, et al., 2002; Zhang, et al., 2002). This interference may contribute to a competitive aspect of the observed mixed-type inhibition.

The structure comparison also revealed a substantial difference between the active-site conformations in the *ba*NadD-***3_02*** and *ba*NadD-NaAD complexes. Moreover, the active-site conformation in the *ba*NadD-***3_02*** complex is more similar to apo-*ba*NadD (rmsd between C_α atoms 0.77 Å) than to the *ba*NadD-NaAD complex (rmsd of 1.32 Å). The major conformational differences occur in the regions that are involved in NaMN binding—that is, residues 42–48 (loop connecting β2 and α2), 105–126 (helix α4), and the loop between β5 and β6 (residues 131–149) (Figure 5B). It is tempting to speculate that, in addition to interfering with NaMN substrate binding, the interactions between the inhibitor and *ba*NadD may partially "lock" the enzyme active site in the catalytically impaired apo-like conformation. This hypothetical mechanism may provide a rationale for the observed, largely noncompetitive mode of inhibition described above.

The *ba*NadD enzyme has a tendency to form a homodimer, as observed in the crystal structure of both apo-form and its complex with substrate (Figure 5C) and as confirmed by size-exclusion chromatography and analytical ultracentrifugation (AUC) (data not shown). Inspection of *ba*NadD-***3_02*** complex crystal packing shows that, although the native dimer interface is preserved, an additional dimer interface, related by a two-fold noncrystallographic symmetry similar to that of the "handshake" dimer observed in *B. subtilis* NadD (Olland, et al., 2002) is also present, resulting in a tetrameric appearance (Figure 5D). The ***3_02*** inhibitor binding site is located at this handshake dimer interface. Because the compound binds at a site between two *ba*NadD monomers related by a pseudo-two-fold symmetry, the two symmetrical orientations of ***3_02*** cannot be distinguished. Therefore, we modeled ***3_02*** in both orientations, each with half occupancy (Figure 5E).

Table 1. Inhibition of Target Enzymes and Antibacterial Activity of Selected Compounds

Compound	Structure	IC_{50}[a] (μM)		MIC_{50}[b] (μM)		
		*ec*NadD	*ba*NadD[c]	*E. coli*	*B. anth*	*B. subt*
3_05	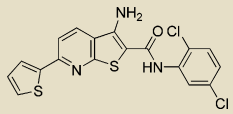	20	9	80	20	10
3_15	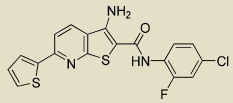	51	12	160	20	30
3_02	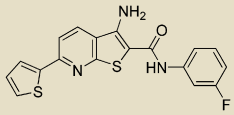	65	36	160	80	80
3_17	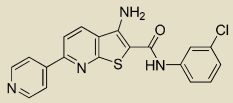	170	>200	80	>160	>160
1_03	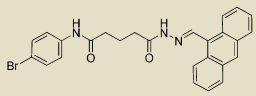	18	33	>80	15	10
1_02	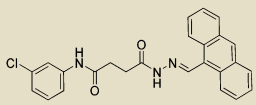	15	25	>80	NA	NA
3_23	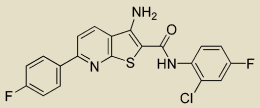	>200	63	40	>80	>80
15_11	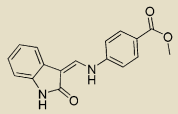	191	98	<100[c]	NA	<50[c]

[a] Inhibitory efficiency of selected compounds (representative of classes 1, 3, and 15) for two target enzymes, *ec*NadD and *ba*NadD, is illustrated by IC_{50} values.

[b] Antibacterial activity of the same compounds against gram-negative (*E. coli*) and gram-positive (*B. subtilis* and *B. anthracis*) model species is reflected by MIC_{50} values (the lowest concentration of compound causing more than 50% growth inhibition). Representative dose-response curves for *B. subtilis* and *B. anthracis* are provided in Figure S4.

[c] Only single-point high estimates of MIC_{50} values were determined (70% growth inhibition at 100 μM for *E. coli*, and 96% inhibition at 50 μM for *B. subtilis*) for a representative of the class 15 that displayed mostly off-target antibacterial activity in *E. coli* model; NA, not assayed.

Although additional interactions between the compound ***3_02*** and the adjacent *ba*NadD subunit at the handshake dimer interface were observed in the crystal structure, it is unlikely that such interactions would contribute to the inhibition observed in our assay conditions. Moreover, AUC data did not reveal any changes in the oligomerization state of the protein in presence of

Table 2. Inhibitory Parameters of Representative Compounds from Two Chemotypes

Inhibitor	***3_02***				***1_02***			
Substrate	NaMN		ATP		NaMN		ATP	
	K_i (μM)	α	K_i (μM)	α	K_i (μM)	α	K_i (μM)	α
*ba*NadD	18 ± 4	2.4	32 ± 5	5.5	9 ± 3	2.3	10 ± 2	2.9
*ec*NadD	25 ± 9	2.5	21 ± 9	2.4	8 ± 3	7.2	5 ± 1	7.1

The apparent values of inhibitory parameters (K_i and α) of two compounds (***3_02*** and ***1_02***) were determined for both enzymes by fitting the kinetic data to the general equation for the mixed-model inhibition (Lyon and Atkins, 2002; see Experimental Procedures for details). The data were collected by varying the concentration of an inhibitor and one of the two substrates (NaMN or ATP) at fixed concentration of another substrate (0.5 mM ATP or NaMN).

the inhibitor. Therefore, the contribution of the handshake dimer interface to *ba*NadD inhibition by ***3_02*** should be negligible under the assay conditions. This conclusion is consistent with the fact that *ec*NadD, being monomeric both in the crystal structure and in solution, exhibits essentially the same inhibitory properties in the presence of ***3_02***, including the same mixed-type mode and similar kinetic parameters.

Notably, the three most flexible regions in *ba*NadD mentioned above also correspond to the regions that deviate the most from the *hs*NMNAT structure (Zhou, et al., 2002) (Figure S2). Comparison of human NMNAT structures (as represented by *hs*NMNAT-1; Zhou, et al., 2002) with various *ba*NadD complexes indicated that *hs*NMNAT active site conformation is much closer to the product-bound conformation of *ba*NadD than to the apo form of *ba*NadD. No significant conformational change has been observed between the apo and ligand bound human NMNAT enzymes (Garavaglia, et al., 2002; Zhang, et al., 2003; Zhou, et al., 2002). Therefore, the active site of *hs*NMNAT, being quite dissimilar from the apo or inhibitor-bound *ba*NadD, appears unable to accommodate or specifically interact with inhibitor ***3_02*** (Figure S2). This interpretation is indirectly supported by the results of comparative virtual docking performed for the three classes of active compounds against *ec*NadD, *ba*NadD, and *hs*NMNAT-1 (see Supplemental Data). The docking energies for the human enzyme consistently have the least favorable scores compared to the energies obtained for *ec*NadD and *ba*NadD, especially in the van der Waals energy terms, suggesting that the overall shape of the binding region in *hs*NMNAT is sufficiently different to allow for selective inhibition of bacterial enzymes.

DISCUSSION

In earlier studies, we used a comparative-genomics approach to identify NAD cofactor biosynthesis as a target pathway for development of new anti-infective therapies (Gerdes, et al., 2002; Osterman and Begley, 2007). The NadD enzyme was chosen as one of the most attractive targets within this pathway because of its nearly universal conservation in bacterial pathogens and because its essentiality was directly confirmed in a number of model bacteria (Gerdes, et al., 2002). A comparative enzymatic and structural analysis revealed substantial differences between bacterial enzymes and their human counterparts, opening an opportunity for development of selective NadD inhibitors. The fact that no drugs are known to act on NadD further contributes to this choice of a target in the context of the growing challenge of multidrug-resistant bacterial pathogens.

In the current study, an integrated structure-based approach was employed to identify small-molecule compounds selectively inhibiting enzymes of the NadD family with a potential broad spectrum of antibacterial activity. By combining computational screening of a virtual compound library with experimental testing of inhibitory and antibacterial activity of selected compounds and their analogs, we have identified and characterized two classes of inhibitors with distinct chemical scaffolds (chemotypes) possessing a number of desired properties (Table 1).

Our approach to in sil*ico* screening was based on selective targeting of those active site residues that are highly conserved among bacterial NadD enzymes, yet quite distinct from the human countertarget enzymes (Zhang, et al., 2002; Zhou, et al., 2002). A focused targeting of a nicotinosyl-binding site (as opposed to an adenosyl-binding site) was also aimed to exploit the functional differences between the NaMN-preferring bacterial NadD and human enzymes with dual specificity for NaMN and NMN substrates (Berger, et al., 2005; Sorci, et al., 2007). We also took advantage of the large conformational differences between the apo and substrate-bound enzymes by specifically targeting the enzyme active site in the apo form so that the inhibitors would stabilize the enzyme in a catalytically impaired conformation.

The obtained results supported the efficiency of this strategy. First, we observed an appreciable correlation between inhibitory properties of compounds against two divergent members of the NadD family, from gram-negative (*ec*NadD) and gram-positive bacteria (*ba*NadD), even at the level of the primary experimental testing of ~300 compounds (Table S1). This trend was even more apparent in the comparison of inhibitory properties of analogs of the three compounds (***1***, ***3***, and ***15***) selected for detailed characterization (Figure 3 and Table S3). These observations indicate that the level of structural conservation in the active sites of divergent representatives of the NadD family provides a potential for developing broad-spectrum inhibitors. At the same time, the three selected chemotypes showed no appreciable activity against human countertargets. This finding validated another premise of this study, that the distinction between bacterial and human enzymes is sufficient for the development of selective (bacterial-specific) NadD inhibitors.

Although the affinity of the best inhibitors identified so far (IC_{50} in 4–30 μM range; see Table 1 and Table S3) is not sufficient for them to be considered as candidate drugs, we were able to use

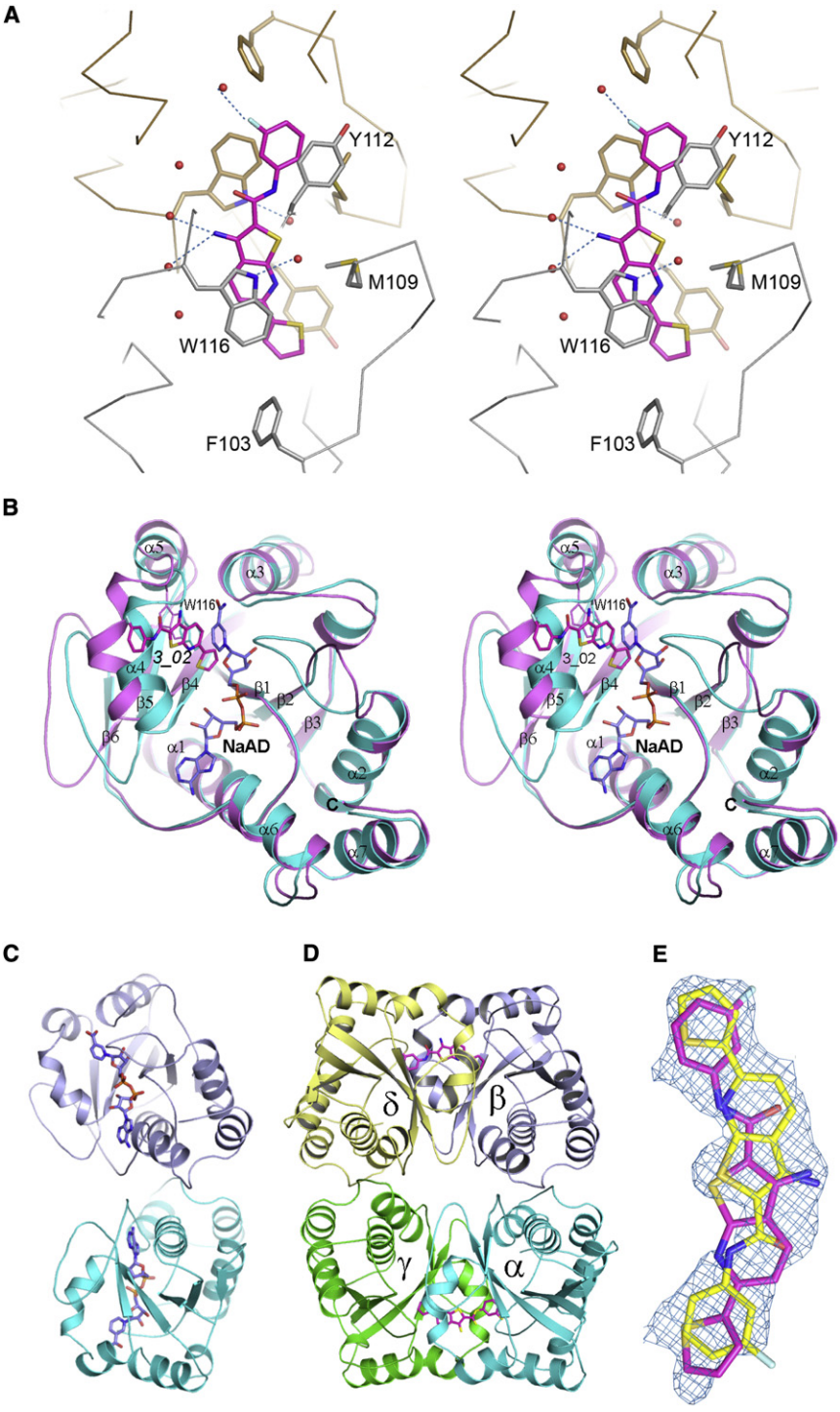

Figure 5. Structure of *ba*NadD in Complex with Inhibitor *3_02* and Comparison with Product-Bound *ba*NadD Structure

(A) Interactions between inhibitor (magenta) and *ba*NadD. The two *ba*NadD monomers are colored gold and gray, respectively. C_α traces of *ba*NadD are shown. Protein residues that interact with ***3_02*** are shown as sticks. Water molecules are shown as small red spheres.

(B) Superimposition of *ba*NadD-NaAD complex structure (cyan) with the inhibitor (***3_02***) bound structure (magenta). The bound product NaAD and inhibitor ***3_02*** are shown as blue and magenta sticks, respectively.

(C) Overall structure of *ba*NadD dimer (cyan and blue subunits) is shown with bound NaAD product. The orientation of this dimer is similar to monomers α and β in Figure 5D.

(D) The tetrameric arrangement of *Bacillus anthracis* NadD-***3_02*** complex in the crystal. Two *ba*NadD dimers are displayed. Only one orientation of the inhibitor ***3_02*** (in sticks) is shown in each binding site.

(E) The *2Fo-Fc* different electron density for the bound inhibitor ***3_02***. The two orientations of the inhibitor are shown in magenta and yellow, respectively.

them as probes to address an important question of NadD target druggability in the cell. The essentiality of the *nadD* gene previously established by genetic techniques does not, by itself, guarantee that inhibition of the NadD enzyme in the cell is possible and may indeed suppress the bacterial growth. Moreover, the antibacterial activity of the analyzed compounds observed in gram-negative (*E. coli*) and gram-positive (*B. subtilis*) model systems (Figure 4), while being encouraging, could be due to some effects other than inhibition of the NadD enzyme. We used an *E. coli* model system to test whether the observed growth suppression was indeed due to the "on-target" action of representative NadD inhibitors. As illustrated in Figures 4C and 4D and Figure S3, overexpression of the target *nadD* gene substantially increased resistance of this strain toward compounds of classes ***1*** and ***3*** (but not ***15***). This finding provided a direct evidence of the on-target action of these compounds, in contrast to the tested compounds of class ***15***, whose antibacterial activity appears to be largely due to unknown off-target effect(s). These data directly validated the NadD enzyme as a drug target amenable to inhibition in the cell, which is leading to growth suppression.

It is important to emphasize that this general conclusion holds true regardless of whether further improvement of the currently selected compounds would or would not produce sufficiently potent antibacterial agents. The major goal of the present study, to assess the druggability of NadD target, dictated the choice of a genetically tractable model system of *E. coli*. Whether the activity of the same compounds against *B. subtilis* is also due to NadD inhibition remains to be tested, especially since the observed type of growth suppression in *B. subtilis* culture is different from that in *E. coli* (growth delay versus decreased final cell density).

Finally, it was important to test the binding mode of NadD inhibitors. This seemed particularly important as the steady-state kinetic analysis of the representative compounds of both classes ***1*** and ***3*** revealed a mixed-type inhibition with a strong noncompetitive component. To assess inhibitor binding mode(s) and to obtain a basis for rational improvement of the inhibitors, we attempted cocrystallization of both bacterial NadD enzymes with a panel of compounds of classes ***1*** and ***3***. The structure of *ba*NadD in complex with the compound ***3_02*** reported here confirmed that this inhibitor indeed binds in the active site area partially overlapping with the targeted NaMN substrate binding site (Figure 5B). The experimentally determined location of the inhibitor is adjacent to that predicted by the in silico docking (Figure S5). Moreover the conformation of the *ba*NadD active site in this complex is drastically different from its product-bound conformation, which is also reported in this study. In fact, the inhibitor binding appears to stabilize the *ba*NadD conformation in its apo form, incompatible with substrate binding and catalysis (Lu, et al., 2008; Sershon, et al., 2009). Inhibitor interference at the level of substrate binding and the stabilization of alternative enzyme conformation may provide a rationale for the observed complex (mixed-type) kinetics of inhibition. Although the actual inhibitory mechanism is not fully clear, the obtained structural information is useful for further inhibitor optimization via structure-based design and synthesis of analogs. For example, engineering additional functional groups that may form specific hydrogen-bond interactions with the enzyme should enhance the binding affinity of the compound.

SIGNIFICANCE

In this study, we have demonstrated the feasibility of developing NadD inhibitors against divergent members of NadD family with strong selectivity for bacterial (versus human) enzymes. Some of the selected inhibitors displayed an appreciable antibacterial activity in both gram-positive and gram-negative model systems. The established "on-target" action of these inhibitors confirmed that NadD is a tractable drug target for the development of novel antibacterial agents. The cocrystal structure of the compound *3_02* in complex with *ba*NadD confirmed its binding at the active site and provided guidelines for inhibitor improvement. These results, taken together, illustrate the power of combining comparative genomics with a structure-based approach for the development of new classes of anti-infective agents.

EXPERIMENTAL PROCEDURES

Materials

All common buffers and reagents were purchased from Sigma-Aldrich. Small molecules selected from in silico screening were obtained from Chembridge, Specs.net and ChemDiv Inc.

In Silico Database Screening

The substrate binding site of *ec*NadD (Zhang, et al., 2002) was selected as the target for docking. System preparation involved analysis of the target protein structure, selection of inhibitor binding site, and generation of the sphere set used to direct the docking (see Supplemental Data for details). All database screening calculations were carried out with DOCK 4.0 (Krumrine, et al., 2003; Kuntz, et al., 1982). The primary screening was performed on a 3D database of over 1 million low-molecular-weight commercially available compounds developed in the University of Maryland Computer-Aided Drug Design (CADD) Center (Huang, et al., 2004; Zhong, et al., 2007). Ligand flexibility was incorporated during docking via the anchor-based search method (Ewing and Kuntz, 1997). Compounds from the initial primary screen were docked onto the protein according to the total ligand-protein interaction energy and were scored on the basis of the van der Waals (vdW) attractive energies normalized for molecular size (Pan, et al., 2003).

Top scoring compounds from the primary screen were subjected to more rigorous secondary docking, where additional optimization of the ligand was performed during the build-up procedure. Additionally, conformational flexibility of *ec*NadD was taken into account via the inclusion of multiple protein conformations either from the crystallographic studies (*secondary screen A*) or from a molecular dynamics (MD) simulation of *ec*NadD (*secondary screen B*). In *secondary screen A*, the top 20,000 scoring compounds from the primary screening were individually docked to the three conformations of apo *ec*NadD obtained from the 1k4k crystal structure. In *secondary screen B*, multiple protein conformations were obtained from the MD simulation of apo *ec*NadD (see Supplemental Data). The top 50,000 scoring compounds from the primary screen were then docked against five MD-generated conformations and were ranked using the normalized total interaction energy for each compound. The top scoring compounds from the two separate secondary screens, totaling 500 and 1000, respectively, were then separately subjected to the final compound selection based on physical properties and chemical similarity. Determination of chemical similarity and further selection of compounds were performed according to standard procedures (Supplemental Data). Finally, a total of 529 unique compounds were selected; of these, 307 were purchased from the commercial vendors for the in vitro inhibition assay. After primary testing (see below), three chemotypes (classes ***1***, ***3***, and ***15***) were selected for further analysis of chemical analogs. A total of 89 analogs were purchased and experimentally tested.

Kinetic Analysis of NadD and Primary Testing of Selected Compounds

A discontinuous assay was utilized to determine the steady-state kinetics parameters k_{cat} and K_m for NadD and for inhibitory testing of selected compounds. This assay couples pyrophosphate (PP_i) byproduct formation of NaMNATase activity to colorimetric detection of free phosphate released upon enzymatic hydrolysis.

(1) NaMN Adenylyltransferase (NaMNATase) reaction

$$NaMN + ATP + Mg^{2+} \rightarrow NaAD^{+} + PP_i + Mg^{2+}$$

(2) Inorganic pyrophosphatase (IPase) reaction

$$PP_i + H_2O \rightarrow 2P_i$$

Excess IPase is used to ensure rapid conversion of pyrophosphate to orthophosphate so that the rate-limiting step in this system is the NaMN adenylyltransferase reaction. Excess inorganic phosphate also decreases the probability that observed inhibition is due to the inhibition of IPase and not the target enzyme. We have since confirmed that the best NadD inhibitors (with IC_{50} values ranging from 5 to 25 μM) did not inhibit IPase.

Steady-state kinetic analysis of *ec*NadD and *ba*NadD target enzymes was performed by varying substrate (NaMN or ATP); concentrations were 0, 10, 30, 60, 200, and 500 μM at fixed saturating concentration of second substrate (0.5 mM). Apparent values of K_m and k_{cat} were calculated by fitting initial rates to a standard Michaelis-Menten model using the software Prism 4 (GraphPad).

The standard inhibition assay was configured in a 96-well format for automated liquid-handling and convenient readout. Each compound was prepared as a 10 mM stock solution in dimethyl sulfoxide (DMSO) and diluted

ten fold (10% DMSO) before usage. Each reaction contained 2.3 nM *ec*NadD (or 1.2 nM *ba*NadD) in 100 mM HEPES (pH 7.5) buffer, 0.2 mM ATP, 0.07 or 0.2 mM NaMN, 10 mM $MgCl_2$, 0.1 mg/ml bovine serum albumin, 0.2 U inorganic pyrophosphatase, and 50 or 100 μM tested compound (the complete lists of tested compounds with structure and vendor information is provided in Tables S1 and S2). Although the use of surfactants is a common practice to reduce the effects of promiscuous inhibitors, an observed interference of Triton X-100 at 0.01% with our assay prompted us to include bovine serum albumin (0.1–1 mg/ml) in the assay mixture to prevent the selection of promiscuous aggregating inhibitors (Coan and Shoichet, 2007). The choice of two-fold $K_{m(app)}$ concentrations of both NaMN and ATP substrates was necessary to ensure a good signal-to-noise ratio under the initial velocity phase of enzymatic reactions (10%–20% substrate depletion), while retaining a linear signal response (0–15 μM PPi). The same assay setup was applied when testing small-molecule inhibitors against human countertargets. Concentrations of *hs*NMNAT-1 and *hs*NMNAT-2 were 3 nM, whereas *hs*NMNAT-3 was tested at 15 nM. After preincubation of the enzyme with the compounds for 5 min at room temperature, the reaction was initiated by addition of NaMN substrate. The reaction was allowed to progress for 20 min at room temperature prior to quenching by addition of 100 μl of malachite green reagent in 1.2 M sulfuric acid prepared as described by Cogan, et al. (1999). After 20–30 min incubation to allow for complex/color formation, the absorbance in each well was measured at 620 nm using a microplate reader (Beckman DTX-880). To account for contribution of free Pi and/or PPi (present in the sample or released due to nonspecific hydrolysis of ATP during incubation) as well as of background absorbance (color) of the tested compounds, parallel reactions were run for each experimental point without addition of NadD enzymes, and their OD_{620} values were subtracted from the measurements of enzyme activity in their respective samples. Reaction in the presence of 2% DMSO but without inhibitory compound served as a positive control. Each measurement was made in triplicate. On the basis of the sensitivity and reproducibility of the assay, inhibition ≥20% was considered reliable. A continuous coupled assay that detected reduction of NAD^+ (Kurnasov, et al., 2002) was used for preliminary assessment of NaMNTase activity and to corroborate kinetic parameters obtained with malachite green discontinuous assay.

IC_{50} Measurements and K_i Determination

The compounds selected on the basis of the results of primary testing were further characterized using the malachite green end-point assay. The initial rate of enzymatic reaction was measured at fixed NaMN and ATP concentrations (equal to two-fold K_m values) and various concentrations of an inhibitory compound. The IC_{50} value was determined by plotting the relative NaMNATase activity versus inhibitor concentration and fitting to the equation *(1)* using GraphPad Prism®.

$$V_i = \frac{V_0}{1 + \frac{[I]}{IC_{50}}} \quad (1)$$

V_0 and V_i represent initial rates in the absence and presence of inhibitor concentration [I].

For K_i determination, the enzyme was preincubated with various fixed concentrations of inhibitors for 5 min. The reaction was initiated by the addition of fixed concentration of NaMN (five-fold K_m) at varying concentrations of ATP (ranging from 0.2 to five-fold K_m) and vice versa. The inhibition constant and inhibition pattern were evaluated by fitting the data to the Michealis-Menten rate equation *(2)* for general (mixed-type) inhibition (Lyon and Atkins, 2002) with the program GraphPad Prism®.

$$V = \frac{V_{max}[S]}{K_m\left(1 + \frac{[I]}{K_i}\right) + [S]\left(1 + \frac{[I]}{\alpha K_i}\right)} \quad (2)$$

V_{max} and K_m are standard Michaelis-Menten parameters, and K_i is the equilibrium dissociation constant for the enzyme-inhibitor complex. The parameter α defines the degree to which the inhibitor binding affects the affinity of the enzyme for the substrate and is diagnostic of the inhibition mode, which may be purely competitive ($\alpha >> 1$), purely noncompetitive ($\alpha = 1$), uncompetitive ($\alpha << 1$), or mixed-type ($\alpha > 1$ or $\alpha < 1$).

Suppression of Bacterial Growth in Culture

Diagnostic *E. coli* strains used for growth-suppression experiments and for target verification were prepared in the background of the *E. coli* K-12 BW25113 (Δ*nadA*) knockout strain with disrupted NAD de novo synthesis pathway from the Keio collection (a gift by Dr. H. Mori, Keio University, Japan) (Baba, et al., 2006). This strain was used in combination with one of the two expression plasmids from the *E. coli* ASKA library (Kitagawa, et al., 2005) enabling inducible overexpression of (1) the *E. coli nadD* gene (to test for the increased resistance against NadD inhibitors) or (2) the *E. coli gapA* gene, a housekeeping metabolic enzyme glyceraldehyde-3-phosphate dehydrogenase (as a negative control). Starter cultures were grown overnight in LB medium. Cells were harvested, washed, and resuspended in the M9 minimal growth medium containing 1% glycerol, 0.1 mM IPTG, 50 mg/l kanamicin, 35 mg/l chloramphenicol, and a limiting amount of nicotinamide (Nam, 0.4 μM). Upon reaching an optical density at 600 nm of 0.05, cells were used to initiate growth experiments in 96-well plate at various concentrations of inhibitors.

The bacterial growth at 37°C in these (and other) experiments was monitored by continuous absorbance measurement at 600 nm using an orbital shaker/microplate reader ELx808™. The area under the growth curve (AUGC) was used to calculate the growth inhibition (Firsov, et al., 2001) and was compared to the respective amount of DMSO. The AUGC was integrated and calculated with GraphPad Prism 4. Growth suppression studies of *B. subtilis* 168 (Bs168) were performed following a similar procedure in a chemically defined medium (Rodionov, et al., 2009) containing glucose (4 g/l), tryptophan (50 mg/l), glutamine (2 g/l), K_2HPO_4 (10 g/l), KH_2PO_4 (6 g/l), sodium citrate (1 g/l), $MgSO_4$ (0.2 g/l), K_2SO_4 (2 g/l), $FeCl_3$ (4 mg/l), and $MnSO_4$ (0.2 mg/l). *B. anthracis* was grown in the same minimal medium containing additionally 10% LB medium for robust growth.

Selected compounds causing an appreciable growth inhibition were subjected to minimal inhibitory concentration (MIC) determination in a series of dilutions from 160 μM down to 2.5 μM. The high concentration limit was determined by solubility problems observed for many compounds. In this concentration range, only some of the analyzed compounds displayed >90% growth inhibition. Therefore, for consistency, the value of MIC was defined as the lowest concentration of compound that caused more than 50% growth inhibition (as determined by AUGC method).

Purification and Crystallography

The expression and purification of *ec*NadD and *ba*NadD were performed as described elsewhere (Zhang, et al., 2002). The human proteins *hs*NMNAT-1, *hs*NMNAT-2, and *hs*NMNAT-3 were also expressed in *E.* and purified as reported elsewhere (Gerdes, et al., 2002; Zhang, et al., 2003; Zhou, et al., 2002). For crystallization, *ba*NadD was first purified with Ni Sepharose HP column (GE Healthcare) and treated with TEV protease overnight before being passed through the Ni column again to remove the 6xHis tag. The tag-free protein was further purified by a Resource Q anion exchange column and Superdex 75 16/60 gel filtration column (GE Healthcare). The purified protein was concentrated to 20 mg/ml before crystallization. The *ba*NadD-NaAD complex crystal was obtained in a hanging drop vapor diffusion setup in the presence of 10 mM NaAD at 20°C. The reservoir contained 20% PEG 3350 and 0.2 M calcium acetate. The cocrystals of *ba*NadD with compound ***3_02*** were obtained in the presence of 1 mM ***3_02*** in conditions similar to those for the NaAD complex crystals. Before data collection, the *ba*NadD-NaAD cocrystals were transferred to a cryoprotectant solution containing 40% PEG 3350 and 0.2 M calcium acetate before being frozen in liquid nitrogen. The *ba*NadD-***3_02*** cocrystals were not stable in such a cryoprotectant solution; therefore, a different cryprotectant containing 20% PEG 3350, 0.2 M calcium acetate, and 15% DMSO was used to stabilize the inhibitor complex crystals before freezing them liquid nitrogen. The X-ray diffraction data were collected on a RAXIS IV^{2+} image plate detector with a FR-E Superbright X-ray generator coupled with Osmic VariMax optics. The data were processed with HKL2000 package (Otwinowski and Minor, 1997). The *ba*NadD-NaAD complex structure was first determined by the molecular replacement methods in the CNS package (Brunger, et al., 1998) using the *B. subtilis* NadD structure (Olland, et al., 2002) as the initial search model (pdb code 1kam). The *ba*NadD inhibitor complex was subsequently solved with molecular-replacement methods, as implemented in the program Molrep (Vagin

Table 3. Crystal Data and Refinement Statistics

Data sets	*ba*NadD·product	*ba*NadD·***3_02***
Data Statistics		
Space group	$P2_12_12_1$	$P2_12_12$
Unit cell (Å)	*a = 41.8, b = 137.41, c = 143.97*	*a = 88.79, b = 97.53, c = 44.30*
Resolution (Å)	50–2.2	50–2.0
Total observations	157926	113171
Unique Reflections	43353	26467
Completeness (outer shell) (%)	98.8 (89.9)	99.9 (100.0)
R_{sym} (outer shell)[a]	0.085 (0.555)	0.037 (0.279)
I/δ (outer shell)	15.9 (2.0)	36.8 (5.4)
Refinement		
R_{work}[b]	0.206	0.205
R_{free}[c]	0.276	0.266
Rmsd bond length (Å)	0.011	0.012
Rmsd bond angle (°)	1.49	1.44
Monomers/asymmetric unit	4	2
Protein atoms	6196	3102
Water molecules	494	309
Ligand atoms	180	53
Average B-factors (Å^2)		
Protein	32.4	28.0
Ligands	24.4	41.1
Water	39.9	34.4
Ramachandran Plot		
Favored region (%)	97.0	98.7
Allowed region (%)	99.3	100.0

[a] $R_{sym} = \Sigma_{hkl} \Sigma_j |I_j - < I > | / \Sigma_{hkl} \Sigma_j |I_j|$.
[b] $R_{work} = \Sigma_{hkl} |F_o - F_c| / \Sigma_{hkl} |F_o|$, where F_o and F_c are the observed and calculated structure factors, respectively.
[c] Five percent randomly selected reflections were excluded from refinement and used in the calculation of R_{free}.

and Teplyakov, 2000), using the *ba*NadD product complex structure (excluding the NaAD ligand) as the search model. Both structures were refined with REFMAC (Murshudov, et al., 1997) in the CCP4 package (CCP4, 1994) and were deposited in the Protein Data Bank with accession codes 3E27 and 3HFJ, respectively. The data collection and refinement statistics for both structures are listed in Table 3. The models were analyzed by MolProbity program (Lovell, et al., 2003).

Analytical Ultracentrifugation

Sedimentation equilibrium experiments were performed in a ProteomeLab XL-I (BeckmanCoulter) analytical ultracentrifuge. Protein samples at 0.22 mg/ml concentration were loaded in 6-channel equilibrium cells and spun in an An-50 Ti 8-place rotor at 15,000 and 18,000 rpm, at 20°C for 24 hr for each speed. The sample buffer contained 20 mM HEPES (pH 7.4) and 5% DMSO. Small-molecule inhibitors were tested at 50 μM. Absorbance profiles were acquired at 280 nm and analyzed with HeteroAnalysis software (National Analytical Ultracentrifugation Facility at the University of Connecticut). Apparent molecular weight (Mw) was determined by fitting the experimental data with the Ideal equilibrium model. If the apparent Mw was higher than calculated theoretical Mw for the monomer, the data were fitted using Monomer-Nmer or Monomer-Nmer-Mmer equilibrium models.

ACCESSION NUMBERS

Coordinates have been deposited in the Protein Data Bank with accession codes 3E27 and 3HFJ.

SUPPLEMENTAL DATA

Supplemental data includes five figures, three tables, and Supplemental Experimental Procedures and can be found with this article online at http://www.cell.com/chemistry-biology/supplemental/S1074-5521(09)00216-6.

ACKNOWLEDGMENTS

This work was supported by the NIAID grant AI059146 "Targeting cofactor biosynthesis in biodefense pathogens" to AO and HZ. A. M. acknowledges the support from the University of Maryland Computer-Aided Drug Design Center. We thank Darek Martynowski for help with X-ray diffraction data collection, Andrey Bobkov at the Protein Production and Analysis Facility of BIMR for AUC analysis, Marat Kazanov and Ying Zhang for data processing.

Received: March 30, 2009
Revised: July 8, 2009
Accepted: July 15, 2009
Published: August 27, 2009

REFERENCES

Baba, T., Ara, T., Hasegawa, M., Takai, Y., Okumura, Y., Baba, M., Datsenko, K.A., Tomita, M., Wanner, B.L., and Mori, H. (2006). Construction of *Escherichia coli* K-12 in-frame, single-gene knockout mutants: the Keio collection. Mol. Syst. Biol. *2*, 2006.0008.

Berger, F., Lau, C., Dahlmann, M., and Ziegler, M. (2005). Subcellular compartmentation and differential catalytic properties of the three human nicotinamide mononucleotide adenylyltransferase isoforms. J. Biol. Chem. *280*, 36334–36341.

Bonnac, L., Chen, L., Pathak, R., Gao, G., Ming, Q., Bennett, E., Felczak, K., Kullberg, M., Patterson, S.E., Mazzola, F., et al. (2007). Probing binding requirements of NAD kinase with modified substrate (NAD) analogues. Bioorg. Med. Chem. Lett. *17*, 1512–1515.

Boshoff, H.I., Xu, X., Tahlan, K., Dowd, C.S., Pethe, K., Camacho, L.R., Park, T.H., Yun, C.S., Schnappinger, D., Ehrt, S., et al. (2008). Biosynthesis and recycling of nicotinamide cofactors in mycobacterium tuberculosis. An essential role for NAD in nonreplicating bacilli. J. Biol. Chem. *283*, 19329–19341.

Brunger, A.T., Adams, P.D., Clore, G.M., DeLano, W.L., Gros, P., Grosse-Kunstleve, R.W., Jiang, J.S., Kuszewski, J., Nilges, M., Pannu, N.S., et al. (1998). Crystallography & NMR system: A new software suite for macromolecular structure determination. Acta Crystallogr. D Biol. Crystallogr. *54*, 905–921.

Butina, D. (1999). Unsupervised data base clustering based on Daylight's Fingerprint and Tanimoto Similarity: a fast and automated way to cluster small and large data sets. J. Chem. Inf. Comput. Sci. *39*, 747–750.

Chen, L., Petrelli, R., Felczak, K., Gao, G., Bonnac, L., Yu, J.S., Bennett, E.M., and Pankiewicz, K.W. (2008). Nicotinamide adenine dinucleotide based therapeutics. Curr. Med. Chem. *15*, 650–670.

Coan, K.E., and Shoichet, B.K. (2007). Stability and equilibria of promiscuous aggregates in high protein milieus. Mol. Biosyst. *3*, 208–213.

Cogan, E.B., Birrell, G.B., and Griffith, O.H. (1999). A robotics-based automated assay for inorganic and organic phosphates. Anal. Biochem. *271*, 29–35.

CCP4 (Collaborative Computational Project, Number 4). (1994). The CCP4 suite: programs for protein crystallography. Acta Crystallogr. D Biol. Crystallogr. *50*, 760–763.

Ewing, T.J.A., and Kuntz, I.D. (1997). Critical evaluation of search algorithms for automated molecular docking and database screening. J. Comp. Chem. *18*, 1175–1189.

Firsov, A.A., Lubenko, I.Y., Portnoy, Y.A., Zinner, S.H., and Vostrov, S.N. (2001). Relationships of the area under the curve/MIC ratio to different integral

endpoints of the antimicrobial effect: gemifloxacin pharmacodynamics in an in vitro dynamic model. Antimicrob. Agents Chemother. *45*, 927–931.

Garavaglia, S., D'Angelo, I., Emanuelli, M., Carnevali, F., Pierella, F., Magni, G., and Rizzi, M. (2002). Structure of human NMN adenylyltransferase. A key nuclear enzyme for NAD homeostasis. J. Biol. Chem. *277*, 8524–8530.

Gerdes, S., Edwards, R., Kubal, M., Fonstein, M., Stevens, R., and Osterman, A. (2006). Essential genes on metabolic maps. Curr. Opin. Biotechnol. *17*, 448–456.

Gerdes, S.Y., Scholle, M.D., D'Souza, M., Bernal, A., Baev, M.V., Farrell, M., Kurnasov, O.V., Daugherty, M.D., Mseeh, F., Polanuyer, B.M., et al. (2002). From genetic footprinting to antimicrobial drug targets: examples in cofactor biosynthetic pathways. J. Bacteriol. *184*, 4555–4572.

Gerlach, G., and Reidl, J. (2006). NAD+ utilization in Pasteurellaceae: simplification of a complex pathway. J. Bacteriol. *188*, 6719–6727.

Godden, J.W., Stahura, F.L., and Bajorath, J. (2005). Anatomy of fingerprint search calculations on structurally diverse sets of active compounds. J. Chem. Inf. Model. *45*, 1812–1819.

Han, S., Forman, M.D., Loulakis, P., Rosner, M.H., Xie, Z., Wang, H., Danley, D.E., Yuan, W., Schafer, J., and Xu, Z. (2006). Crystal structure of nicotinic acid mononucleotide adenylyltransferase from *Staphyloccocus aureus*: structural basis for NaAD interaction in functional dimer. J. Mol. Biol. *360*, 814–825.

Huang, N., Nagarsekar, A., Xia, G., Hayashi, J., and MacKerell, A.D., Jr. (2004). Identification of non-phosphate-containing small molecular weight inhibitors of the tyrosine kinase p56 Lck SH2 domain via in silico screening against the pY + 3 binding site. J. Med. Chem. *47*, 3502–3511.

Khan, J.A., Forouhar, F., Tao, X., and Tong, L. (2007). Nicotinamide adenine dinucleotide metabolism as an attractive target for drug discovery. Expert Opin. Ther. Targets *11*, 695–705.

Kitagawa, M., Ara, T., Arifuzzaman, M., Ioka-Nakamichi, T., Inamoto, E., Toyonaga, H., and Mori, H. (2005). Complete set of ORF clones of *Escherichia coli* ASKA library (a complete set of *E. coli* K-12 ORF archive): unique resources for biological research. DNA Res. *12*, 291–299.

Krumrine, J., Raubacher, F., Brooijmans, N., and Kuntz, I. (2003). Principles and methods of docking and ligand design. Methods Biochem. Anal. *44*, 443–476.

Kuntz, I.D., Blaney, J.M., Oatley, S.J., Langridge, R., and Ferrin, T.E. (1982). A geometric approach to macromolecule-ligand interactions. J. Mol. Biol. *161*, 269–288.

Kurnasov, O.V., Polanuyer, B.M., Ananta, S., Sloutsky, R., Tam, A., Gerdes, S.Y., and Osterman, A.L. (2002). Ribosylnicotinamide kinase domain of NadR protein: identification and implications in NAD biosynthesis. J. Bacteriol. *184*, 6906–6917.

Lau, C., Niere, M., and Ziegler, M. (2009). The NMN/NaMN adenylyltransferase (NMNAT) protein family. Front. Biosci. *14*, 410–431.

Lovell, S.C., Davis, I.W., Arendall, W.B., 3rd, de Bakker, P.I., Word, J.M., Prisant, M.G., Richardson, J.S., and Richardson, D.C. (2003). Structure validation by Calpha geometry: phi,psi and Cbeta deviation. Proteins *50*, 437–450.

Lu, S., Smith, C.D., Yang, Z., Pruett, P.S., Nagy, L., McCombs, D., Delucas, L.J., Brouillette, W.J., and Brouillette, C.G. (2008). Structure of nicotinic acid mononucleotide adenylyltransferase from *Bacillus anthracis*. Acta. Crystallogr. Sect. F. Struct. Biol. Cryst. Commun. *64*, 893–898.

Lyon, R.P., and Atkins, W.M. (2002). Kinetic characterization of native and cysteine 112-modified glutathione S-transferase A1-1: reassessment of non-substrate ligand binding. Biochemistry *41*, 10920–10927.

Magni, G., Orsomando, G., Raffelli, N., and Ruggieri, S. (2008). Enzymology of mammalian NAD metabolism in health and disease. Front. Biosci. *13*, 6135–6154.

Magni, G., Di Stefano, M., Orsomando, G., Raffaelli, N., and Ruggieri, S. (2009). NAD(P) biosynthesis enzymes as potential targets for selective drug design. Curr. Med. Chem. *16*, 1372–1390.

McDevitt, D., and Rosenberg, M. (2001). Exploiting genomics to discover new antibiotics. Trends Microbiol. *9*, 611–617.

Moro, W.B., Yang, Z., Kane, T.A., Brouillette, C.G., and Brouillette, W.J. (2009). Virtual screening to identify lead inhibitors for bacterial NAD synthetase (NADs). Bioorg. Med. Chem. Lett. *19*, 2001–2005.

Murshudov, G.N., Vagin, A.A., and Dodson, E.J. (1997). Refinement of macromolecular structures by the maximum-likelihood method. Acta Crystallogr. D Biol. Crystallogr. *53*, 240–255.

Olland, A.M., Underwood, K.W., Czerwinski, R.M., Lo, M.C., Aulabaugh, A., Bard, J., Stahl, M.L., Somers, W.S., Sullivan, F.X., and Chopra, R. (2002). Identification, characterization, and crystal structure of *Bacillus subtilis* nicotinic acid mononucleotide adenylyltransferase. J. Biol. Chem. *277*, 3698–3707.

Osterman, A.L., and Begley, T.P. (2007). A subsystems-based approach to the identification of drug targets in bacterial pathogens. Prog. Drug Res. *64*, 131–, 133–170.

Otwinowski, Z., and Minor, W. (1997). Processing of X-ray diffraction data collected in oscillation mode. In Methods in Enzymology, C.W. Carter, Jr. and R.M. Sweet, eds. (London: Academic Press), pp. 307–326.

Pan, Y., Huang, N., Cho, S., and MacKerell, A.D., Jr. (2003). Consideration of molecular weight during compound selection in virtual target-based database screening. J. Chem. Inf. Comput. Sci. *43*, 267–272.

Poncet-Montange, G., Assairi, L., Arold, S., Pochet, S., and Labesse, G. (2007). NAD kinases use substrate-assisted catalysis for specific recognition of NAD. J. Biol. Chem. *282*, 33925–33934.

Rodionov, D.A., Hebbeln, P., Eudes, A., ter Beek, J., Rodionova, I.A., Erkens, G.B., Slotboom, D.J., Gelfand, M.S., Osterman, A.L., Hanson, A.D., et al. (2009). A novel class of modular transporters for vitamins in prokaryotes. J. Bacteriol. *191*, 42–51.

Sassetti, C.M., Boyd, D.H., and Rubin, E.J. (2003). Genes required for mycobacterial growth defined by high density mutagenesis. Mol. Microbiol. *48*, 77–84.

Sershon, V.C., Santarsiero, B.D., and Mesecar, A.D. (2009). Kinetic and X-ray structural evidence for negative cooperativity in substrate binding to nicotinate mononucleotide adenylyltransferase (NMAT) from *Bacillus anthracis*. J. Mol. Biol. *385*, 867–888.

Shoichet, B.K. (2006). Screening in a spirit haunted world. Drug Discov. Today *11*, 607–615.

Sorci, L., Cimadamore, F., Scotti, S., Petrelli, R., Cappellacci, L., Franchetti, P., Orsomando, G., and Magni, G. (2007). Initial-rate kinetics of human NMN-adenylyltransferases: substrate and metal ion specificity, inhibition by products and multisubstrate analogues, and isozyme contributions to NAD+ biosynthesis. Biochemistry *46*, 4912–4922.

Sorci, L., Martynowski, D., Rodionov, D.A., Eyobo, Y., Zogaj, X., Klose, K.E., Nikolaev, E.V., Magni, G., Zhang, H., and Osterman, A.L. (2009). Nicotinamide mononucleotide synthetase is the key enzyme for an alternative route of NAD biosynthesis in *Francisella tularensis*. Proc. Natl. Acad. Sci. USA *106*, 3083–3088.

Vagin, A., and Teplyakov, A. (2000). An approach to multi-copy search in molecular replacement. Acta Crystallogr. D Biol. Crystallogr. *56*, 1622–1624.

Velu, S.E., Cristofoli, W.A., Garcia, G.J., Brouillette, C.G., Pierson, M.C., Luan, C.H., DeLucas, L.J., and Brouillette, W.J. (2003). Tethered dimers as NAD synthetase inhibitors with antibacterial activity. J. Med. Chem. *46*, 3371–3381.

Velu, S.E., Luan, C.H., Delucas, L.J., Brouillette, C.G., and Brouillette, W.J. (2005). Tethered dimer inhibitors of NAD synthetase: parallel synthesis of an aryl-substituted SAR library. J. Comb. Chem. *7*, 898–904.

Velu, S.E., Mou, L., Luan, C.H., Yang, Z.W., DeLucas, L.J., Brouillette, C.G., and Brouillette, W.J. (2007). Antibacterial nicotinamide adenine dinucleotide synthetase inhibitors: amide- and ether-linked tethered dimers with alpha-amino acid end groups. J. Med. Chem. *50*, 2612–2621.

Yoon, H.J., Kim, H.L., Mikami, B., and Suh, S.W. (2005). Crystal structure of nicotinic acid mononucleotide adenylyltransferase from *Pseudomonas aeruginosa* in its Apo and substrate-complexed forms reveals a fully open conformation. J. Mol. Biol. *351*, 258–265.

Zhang, H., Zhou, T., Kurnasov, O., Cheek, S., Grishin, N.V., and Osterman, A. (2002). Crystal structures of *E. coli* nicotinate mononucleotide adenylyltransferase and its complex with deamido-NAD. Structure *10*, 69–79.

Zhang, X., Kurnasov, O.V., Karthikeyan, S., Grishin, N.V., Osterman, A.L., and Zhang, H. (2003). Structural characterization of a human cytosolic NMN/NaMN adenylyltransferase and implication in human NAD biosynthesis. J. Biol. Chem. *278*, 13503–13511.

Zhong, S., Macias, A.T., and MacKerell, A.D., Jr. (2007). Computational identification of inhibitors of protein-protein interactions. Curr. Top. Med. Chem. *7*, 63–82.

Zhou, T., Kurnasov, O., Tomchick, D.R., Binns, D.D., Grishin, N.V., Marquez, V.E., Osterman, A.L., and Zhang, H. (2002). Structure of human nicotinamide/nicotinic acid mononucleotide adenylyltransferase. Basis for the dual substrate specificity and activation of the oncolytic agent tiazofurin. J. Biol. Chem. *277*, 13148–13154.

